Crimson Publishers
Wings to the Research

Research Article

A Study on Synthesis, Structural and Magnetic Properties of La_2O_3 Doped Isotropic Ba-M Ferrites

Zubair Ahmad[1]* Shakir Khan[1] and Shan Tao[2]

[1]Ibn-e-Sina Institute of Technology, Pakistan

[2]Magnetism Key Laboratory of Zhejiang Province, China Jiliang University, Hangzhou, China

ISSN: 2576-8840

***Corresponding author:** Zubair Ahmad, Ibn-e-Sina Institute of Technology, Sector H-11/4, Islamabad, Pakistan

Submission: July 13, 2020

Published: August 13, 2020

Volume 13 - Issue 5

How to cite this article: Zubair Ahmad, Shakir Khan, Shan Tao. A Study on Synthesis, Structural and Magnetic Properties of La_2O_3 Doped Isotropic Ba-M Ferrites. Res Dev Material Sci. 13(5). RDMS.000825. 2020. DOI: 10.31031/RDMS.2020.13.000825

Abstract

Present work reports the synthesis, structural and magnetic properties of $BaFe_{11}O_{17.5}$ and La_2O_3 doped (Ba $La_{0.05}Fe_{11}O_{17.575}$, $BaLa_{0.1}Fe_{11}O_{17.65}$, $BaLa_{0.2}Fe_{11}O_{17.80}$ and $BaLa_{0.3}Fe_{11}O_{17.95}$) ferrites produced through powder metallurgy method with escalated magnetic properties. Phase evaluation, crystal structure, microstructure, and magnetic properties thermomagnetic characteristics for the La doped and La free ferrites have been investigated at varying sintered temperatures. XRD studies revealed that $BaFe_{12}O_{19}$ phase is formed at 900 °C through the reaction of Fe_2O_3 and $BaFe_2O_4$. Electron microscopy studies elucidated that microstructural features depend critically on the heat treatment conditions as well as La content. La addition up to 1.0 mole found to be beneficial to refine particle size close to single domain wall size, which, in turn, led to enhance magnetic properties of the ferrite. Optimum magnetic properties for the La free $BaFe_{11}O_{17.5}$ are H_c=4.4kOe, B_r=1.9kG, and $(BH)_{max}$=0.85MGOe which were improved to H_c=4.9kOe, B_r=2.4kG and $(BH)_{max}$=1.2MGOe with La_2O_3 additive. The La_2O_3 acts as a grain growth inhibitor and led to enhance high coercivity of 4.9kOe in the ferrite. The dielectric constant and dielectric loss factor decrease monotonically with increasing applied frequency at the constant temperature. Permeability is found to be sensitive to density and microstructural components like grain size and porosity of the sintered ferrites.

Keywords: Isotropic sintered ferrites; Powder metallurgy; Dielectric properties; Magnetic properties; Microstructure

Introduction

Ceramic magnets based on hexa-ferrite phase, $AFe_{12}O_{19}$ with A=Ba, Sr, Pb have revival interest due to their high magneto-crystalline anisotropy, excellent thermal stability, better corrosion resistance, best service temperature as well as economical manufacturing cost [1,2]. These magnets have found their potential applications in motors, generators, recording media, microwave devices and domestic appliances. Ferrites have been extensively produced by powder metallurgy, sole gel, co-precipitation, and combustion techniques [3-6]. Rare earth Sm-Co and Nd-Fe-B based magnets are considered as high-performance magnets compared to ceramic and steel magnets. Recent global crises of rare earth elements have focused the researchers to re-investigate the rare earth free magnet like Ba/Sr ferrites, Fe-Al-Ni-Co-Ti-Cu, Fe-Cr-Co-Mo and Mn-Al-C. Magnetic properties in Ba hexaferrite are sensitive to the microstructure which becomes ideal or non-ideal based on alloy chemistry and synthesis conditions. An ideal microstructure contains phase particle size close to 1μm (close to domain wall thickness) and has homogenous phase distribution with thin grain boundaries to facilitate ferromagnetic exchange coupling, which, in turn, responsible for good magnetic properties. Researchers have adopted compositional modification and process optimization strategies to improve the performance of ferrite magnets.

Substantial improvements have been made in the microstructure and magnetic properties of ferrites by the researchers. Singh et. al [7] developed Ba-M ferrite magnet with micro alloying of rare earth elements (La^{3+}, Nd^{3+} and Sm^{3+}) which results to decrease B_r and increase H_c from 2.87 to 3.34kOe. Transition metals like Co^{3+}, Cu^{2+} and Ti^{3+} [8] have beneficial effects in improving magnetic properties and perfecting microstructure. Nowosielski et al. [9] reported the effect of ball milling and annealing temperature on crystallite size, phase

development and magnetic properties of $BaFe_{12}O_{19}$. Ding et al. [10] prepared barium ferrite with high coercivity, 5.6kOe, by co-precipitation technique. Sozeri et al. [11] studied the effect of La doping on the magnetic properties of $Ba_{1-x}La_xFe_{12}O_{19}$ prepared by ammonium-citrate sol-gel method and attained H_c of 5.73kOe. Studies have shown that ferrite prepared with La^{3+} or Pr^{3+} doping exhibit higher H_c than simple Ba-M ferrite magnets due to higher magneto-crystalline anisotropy [12]. Ghzaiel et al. [13] invoked the effect of Cr^{3+}, Mn^{3+}, Al^{3+} and Bi^{3+} on the magnetic properties of hydrothermally synthesized $BaFe_{11}O_{19}$ and found that Mn^{3+} doped magnet has higher M_s (61.1emu/g) than that of Cr^{3+} (60.3emu/g). Mn doped magnets have attained optimum H_c value of 4.2kOe and $(BH)_{max}$ of 0.94MGOe. Yang et al. [14] synthesized $Sr_{1-x}La_xFe_{12-x}Cu_xO_{19}$ magnets by ceramic process and found that B_r and $(BH)_{max}$ increased by La doping up to x=0.2 moles. However, many scientific issues related to microstructure and magnetic properties remain unsolved. The present work focuses the development of isotropic barium hexaferrite by the powder metallurgy technique with improved microstructure and magnetic properties. The effects of La content on microstructure and magnetic properties were investigated with varying annealing and sintering temperatures and their results are presented and discussed.

Materials and Methods

Stoichiometric precursor of $BaCO_3$ 99% Alfa Aesar, Fe_2O_3 99% Merck and La_2O_3 99% Alfa Aesar in double distilled H_2O was sealed in 500ml stainless steel jars and homogenized using planetary ball milling for 6 hrs. Pre-milled powders were sieved through 60 mesh stainless steel screen and compacted in cylinders of 13mm in diameter and 12mm in length using stainless steel die. Cylindrical samples of $BaFe_{11}O_{17.5}$ were calcined at 800 ºC, 850 ºC, 900 ºC and 950 ºC temperatures for 2.5 hours with respect to CO_2 loss. Likewise, La-substituted Ba-M ferrites were calcined at 900 ºC for 2.5 hours. Calcined samples were ground in pistol and mortar, sieved through 60 mesh screens and milled for 8 hours to promote homogeneity. The aqueous PVA (72k, Merck) binder was used to facilitate high pressure compaction and cracked free sintering. For sintering, cylindrical samples of 13mm in diameters and 12mm in length were compacted at 15MPa pressure to obtain green density of 3.1g/cm^3. Green compacts of La-0.0 ($BaFe_{11}O_{17.5}$) and La substituted Ba-M ferrites were placed on zirconia plate inside a box furnace with debinding rate of 2 ºC/min at 280 ºC for 1.5hrs followed by sintering at 1050 ºC, 1100 ºC, 1150 ºC and 1200 ºC for 1.5hrs at a heating rate of 5 ***ºC***/min and then cooled to room temperature at the natural cooling rate. Dimensional mass densities were measured using standard digital caliper and precise digital weight balance. Crystal structure and magnetic phases were determined by the X-ray diffraction (Siemen D500-XRD) using Cu kα radiation source in the 2θ scan range of 20º to 90º with 0.05º scanning rate. Phases were identified by comparing the peak positions (2θ) and their corresponding intensities (I) with the standard powder diffraction files (PDF) using the Hanawalt method [15]. The observed phase peaks were indexed with standard JCPD cards (JCPD No. 84-757). The mean crystallite sizes were determined from the X-ray line-broadening analysis using the Deby Scherrer's equation [16] after appropriate correction of instrumental broadening.

Phase compositions and microstructure of ferrites were investigated through field emission scanning electron microscopy (FESEM Quanta FEG 450) equipped with energy dispersive spectrometer (EDS). Magnetic properties were measured by plotting hysteresis loops with pulsed field magnetometer (Metis 40kJ-PFM) using 3T applied field at room temperature. Dielectric properties were measured using LCR meter (7600 Quadtech) at room temperature in the frequency range of 100Hz to 10kHz. The permeability was measured with 3255B Precision Magnetic Analyzer in the frequency regime of 10GHz to 120GHz at room temperature using conventional measurement method.

Results and Discussion

Calcination temperature and weight loss

The calcination decomposes $BaCO_3$ to $CO_{2(g)}$ and BaO which reacts with Fe_2O_3 to form mono-ferrite ($BaFe_2O_4$) or Ba-M ferrite.

$$BaCO_3 \rightarrow BaO + CO_2$$

$$BaO + Fe_2O_3 \rightarrow BaFe_2O_4$$

$$BaFe_2O_4 + 5Fe_2O_3 \rightarrow BaFe_{12}O_{19}$$

The actual 3.9% weight loss of $BaFe_{11}O_{17.5}$ (referred as La-0.0) at 900 °C was matched with expected 4% weight loss. At 800 °C to 850 °C calcination temperature regime, a mono-ferrite, $BaFe_2O_4$, phase is formed, whereas, at 900 °C, mono-ferrite phase disappeared and $BaFe_{12}O_{19}$ phase appeared.

X-ray diffraction analysis

XRD patterns as a function of calcination temperature for the La-0.0 is presented Figure 1a. It shows Bragg's peaks for the un-reacted hematite Fe_2O_3 (JCPDS# 73-2234) at 800 ºC. At 850 ºC, barium mono ferrite ($BaFe_2O_4$) predominately produced with minor unreacted hematite Fe_2O_3 phase. However, at 900 ºC calcination, Fe_2O_3 reacted with $BaFe_2O_4$ to produce $BaFe_{12}O_{19}$ as a main Ba-M ferrite phase (JCPD#84-757). Thus, Fe_2O_3 is completely transformed into $BaFe_{12}O_{19}$ phase after calcination at 900 ˚C as evident by the appearance of Bragg's peaks in the XRD pattern corresponding to Ba-M ferrite phases (Figure 1a). Thus, calcination temperature for the ferrite samples was settled as 900 ºC. The calcined samples were subjected to sintering. Figure 1b illustrates XRD patterns for the samples at varying sintering temperature. It seems that Bragg's peak positions and intensities are almost same for all the sintered samples ranging from 1050 to 1200 ºC. The lattice parameters and crystallite sizes for sintered La-0.0 and La doped samples are listed in Table 1. It seems that crystallite size for the La free (La-0.0) sample is higher than La doped samples. The La-0.05 and La-0.1 samples have 16% smaller crystallite sizes compare to La-0.0 sample while La-0.2 and La-0.3 have 7% lower crystallite sizes than La-0.0 sample. The c/a ratio seems to decrease from 3.98 to 3.94 with increasing the La^{3+} doping.

Table 1: Lattice parameters, c/a ratio, cell volume and crystallite size for different La moles composition.

Sample	Lattice Parameters (Å)		c/a Ratio	Cell Volume (nm^3)	Crystallite Size (nm)
	a	c			
La-0.00	5.8952	23.4777	3.982511	0.706	39.86
La-0.05	5.9091	23.5017	3.977205	0.71	33.04
La-0.1	5.9612	23.5294	3.947091	0.713	33.45
La-0.2	5.9612	23.5294	3.947091	0.724	35.3
La-0.3	5.9379	23.5128	3.959784	0.717	36.51

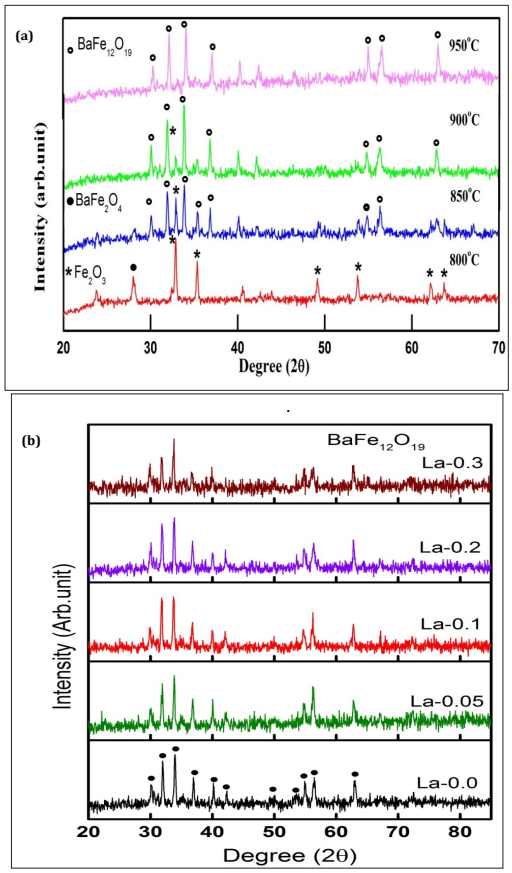

Figure 1: XRD patterns showing magnetic phases as a function of calcination temperatures for La-0.0 samples (a) and (b) XRD patterns for undoped and doped samples sintered at 1100°C.

Microstructural studies

Figure 2a-2c represents FESEM images for Fe_2O_3, La_2O_3 and $BaCO_3$ precursor materials. It shows that Fe_2O_3 has loose particles about 0.7±0.1 µm in size while $BaCO_3$ has agglomerated rod shaped features around 1.5±0.5µm in size (Figure 2b). The La_2O_3 revealed larger sticky particles ranging from 2.5±0.5µm in size as depicted in Figure 2c. In order to attain homogeneity, fine particle size and accelerated solid state diffusion process, precursor powders were subjected to ball milling for 6hrs prior to calcination. Figure 3a-3d represent FESEM images for La-0.0 samples sintered at 1050 ºC, 1100 ºC, 1150 ºC and 1200 ºC for 1.5 hours. Samples sintered at 1050 ºC shows a highly porous, sharp edge grains ranging in size from 0.9±0.3µm with lower density of $4g/cm^3$. A well define sharp edge containing hexagonal grains ranging from 0.7±0.2µm in size are produced at 1100 ºC where a density increments up to 15% was noticed compared to 1050 ºC treated samples. Furthermore, grains are found to be inter-link with neighboring grains that, in turn, enhance the grain coherency and stacking density due to sintering at 1100 ºC. Sintering at 1150 ºC led to enlarge grain sizes whereby hexagonal grains accompanied with rods are formed which had attained mean grain size of 1.7±0.2µm with $4.83g/cm^3$ density (Figure 3c). At 1200 ºC, an excessive grain growth causes grains welding. Thus, optimum sintering temperature for ferrites samples were selected as 1100 ºC by the experimentation.

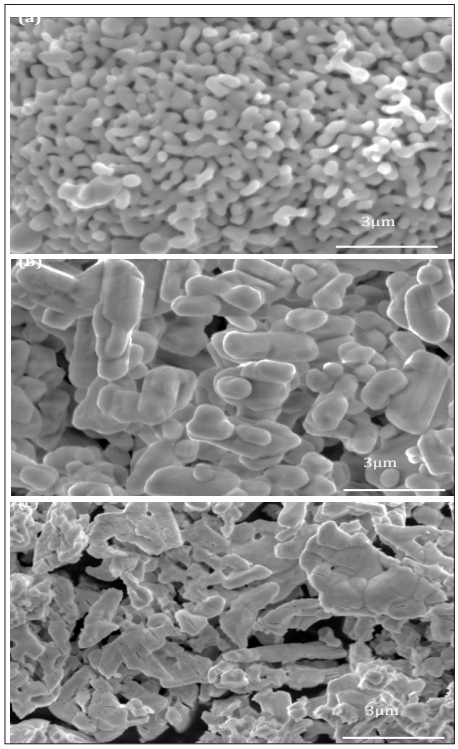

Figure 2:FESEM micrographs showing powder particle morphology of (a) Fe2O3(b) BaCO3and (c) La2O3 precursor material.

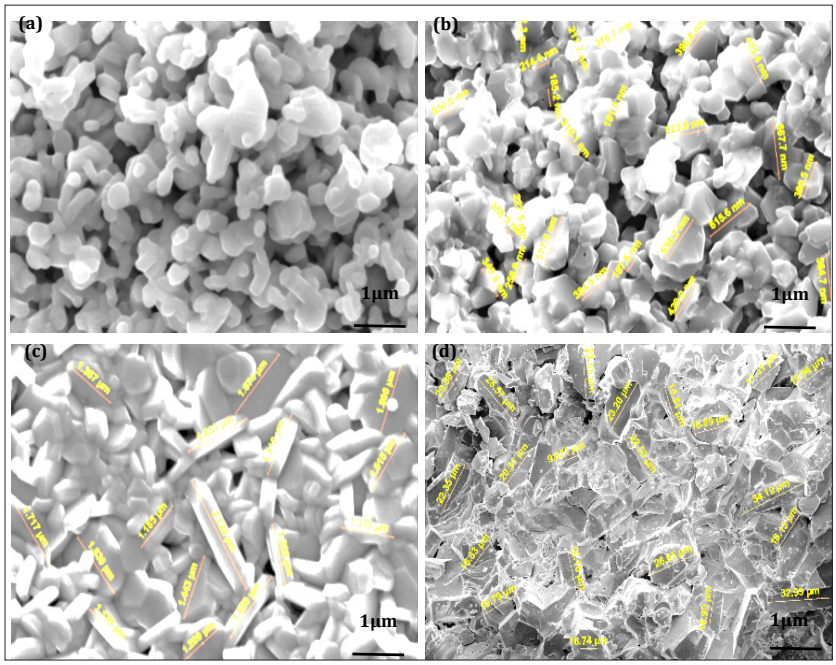

Figure 3: FESEM micrographs showing grains morphology for La-0.0 sample sintered at (a) 1050°C(b) 1100°C (c) 1150°C and (d) 1200°Cfor 1.5 hrs.

FESEM images for La doped ferrites sintered at 1100 °C for 1.5hrs are illustrated in Figure 4. It is evident that La-0.05 microstructure is composed of hexagonal grains around 1.0±0.2µm in size with less porosity. The grain morphology of La-0.10 samples resemble with La-0.05 samples but with a density of 4.5g/cm^3. However, the severity of inter-grain connectivity and degree of grain stacking density is found to be larger for the La-0.1 compared to La-0.05 containing sample. Coarse grains up to 1.4±0.1µm in size were observed for La-0.2 sample. The La-0.3 shows a porous microstructure due to lower density (4.2g/cm^3) with large grain sizes ranging 1.5 to 2µm. SEM studies indicate that La-Ba-M-ferrites have fine grain size and inter grain connectivity with high packing density for the La-0.1 added sample.

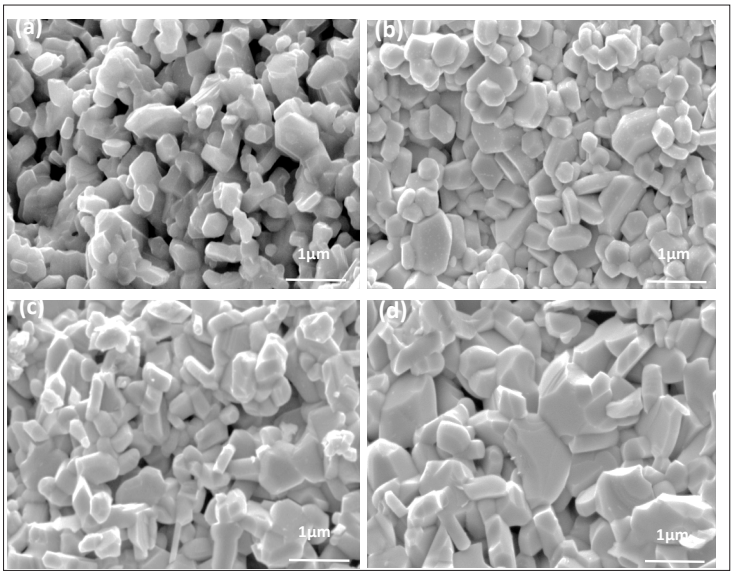

Figure 4:FESEM micrographs showing grain morphology for (a) La-0.05 (b) La-0.1 (c) La-0.2 and (d) La-0.3 doped samples sintered at 1100℃for1.5 hrs.

Magnetic properties

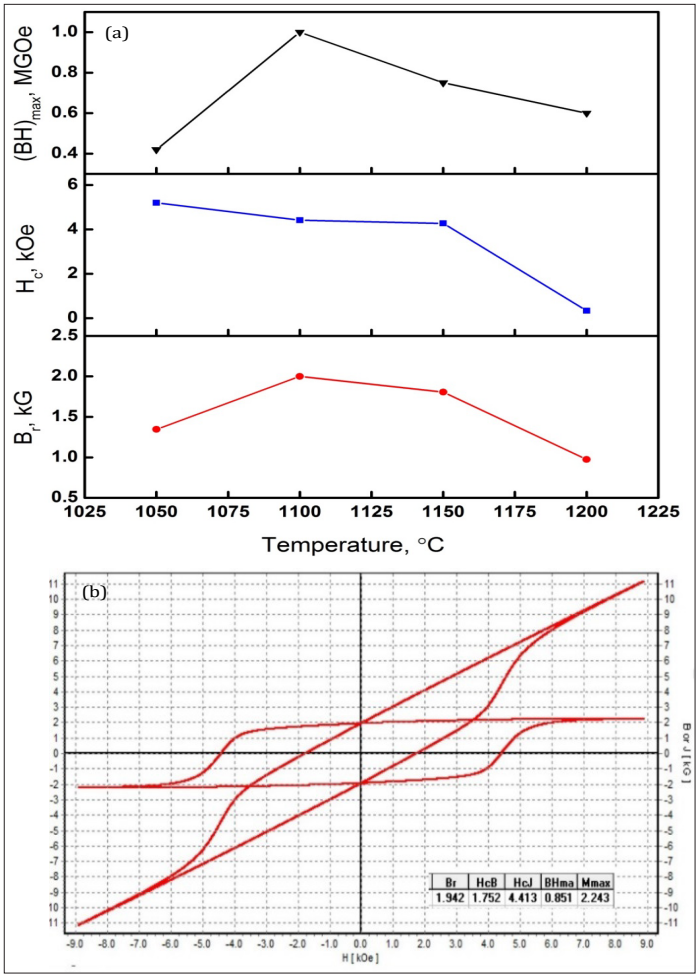

Figure 5: Changes in magnetic properties versus sintering temperature for La-0.0 sample (a) and typical hysteresis loop for La-0.0 sample sintered at 1100°C for 1.5 hrs.

Changes in magnetic properties versus sintering temperature for La-0.0 sample are presented in Figure 5a. It shows that magnetic properties are sensitive to the heat treatment conditions. A small variation from the proper heat treatment conditions may form non ideal microstructure leading to decay in the magnetic parameters. An example, La-0.0 ferrite display a high H_c of 5.0kOe sintered at 1050 ºC, whereas the ferrite sintered at 1100 ºC exhibits a high B_r of 1.9kG. The high H_c is related to fine grain size while high B_r is ascribed from the positive dipole interactions, high grain stacking density as well as optimal density of ferrite. The maximum magnetic properties such as H_c=4.4kOe, B_r=1.9kG, B_s=2.2kG and $(BH)_{max}$=0.85MGOe are obtained for the La-0.0 samples sintered at 1100 ºC as confirmed by plotting the hysteresis loop depicted in Figure 5b. The optimum sintering temperature for La doped samples were selected as 1100 ºC by the experimentations. Figure 6a & 6b illustrates changes in magnetic properties and demagnetization curves as a function of La content sintered at 1100 °C. It shows that both H_c and B_r increases monotonically for La-0.1 and then decreases sharply for the La-0.2 and La-0.3 samples. The best magnetic properties in the series of La doped ferrites were obtained with La-0.1 doped ferrite as H_c=4.9kOe, B_r=2.4kG, B_s=2.26kG and $(BH)_{max}$=1.2MGOe. These magnetic properties are better in comparison with previously reported isotropic bulk and nanosize barium or strontium hexa-ferrite materials [17,18]. These sound properties in present study are ascribed by the fine grain size, homogenous phase grains distribution, high magneto-crystalline anisotropy, less porosity, positive dipole interactions and morphology of hexa-ferrite $BaFe_{12}O_{19}$ phase.

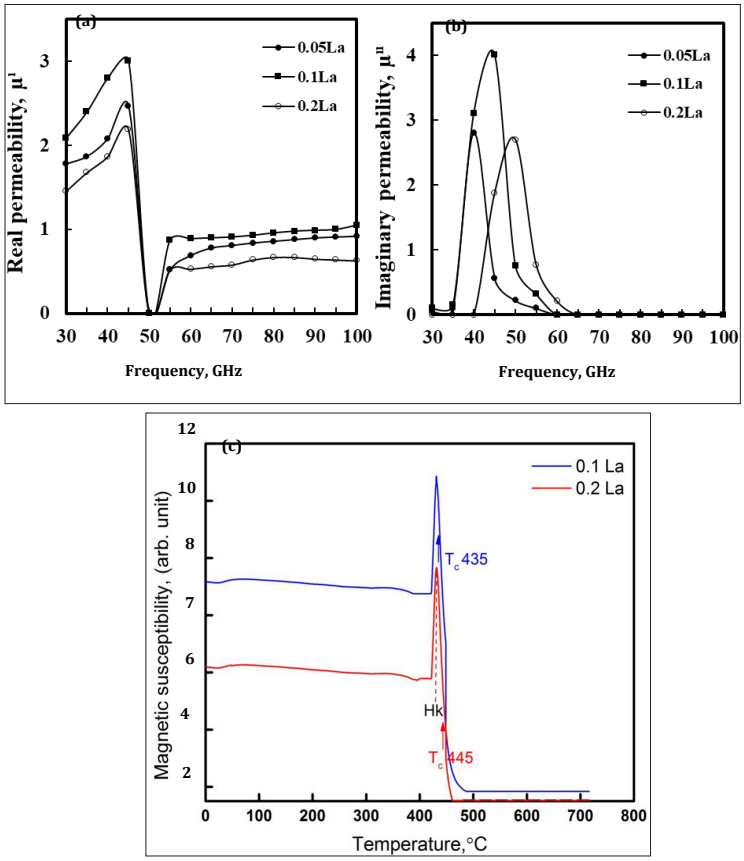

Figure 6: Real part of magnetic permeability (a) imaginary part of magnetic permeability (b) and magnetic susceptibility of La doped ferrites.

Dielectric properties

The dielectric constant for La doped samples were measured as a function of applied frequency ranging 100Hz to 10kHz and defined by the equation [19,20]:

$$\varepsilon = C.H/\varepsilon_o.A \quad (1)$$

Where, ε is dielectric constant, ε_o is permittivity of the free space, C is the capacitance (farads), A = area and H = height of the cylindrical disks.

Figure 7a & 7b presents the variation in dielectric constant and dielectric loss versus applied frequency. In case of La-0.05 sample, a constant fall in dielectric constant and dielectric loss was noticed with increasing applied frequency. The dielectric loss for La-0.5 sample is least at 2kHz frequency and dielectric constant found to be decrease by 92% at 10kHz frequency. A similar variations trend for dielectric constant and dielectric loss with increasing frequency was observed for La-0.1 sample whereby dielectric constant decreased to 98% at 10 kHz. The dielectric constant is further

decreased to 99% for the La-0.2 sample while it was around 84% for La-0.3 doped samples. The decreasing trend of dielectric constant and dielectric loss with the increasing applied frequency can be well explained by the Maxwell model [21,22]. According to the model, the space charge carriers need a finite time to line up their axes in the direction of an applied field. As the applied frequency increases, the electrons turn around their direction of motion more frequently. This causes to decrease the arrival of electrons at the nearby grain boundary and as a result net polarization in the hard ferrite decreases. This decreasing polarization causes the dielectric constant to fall.

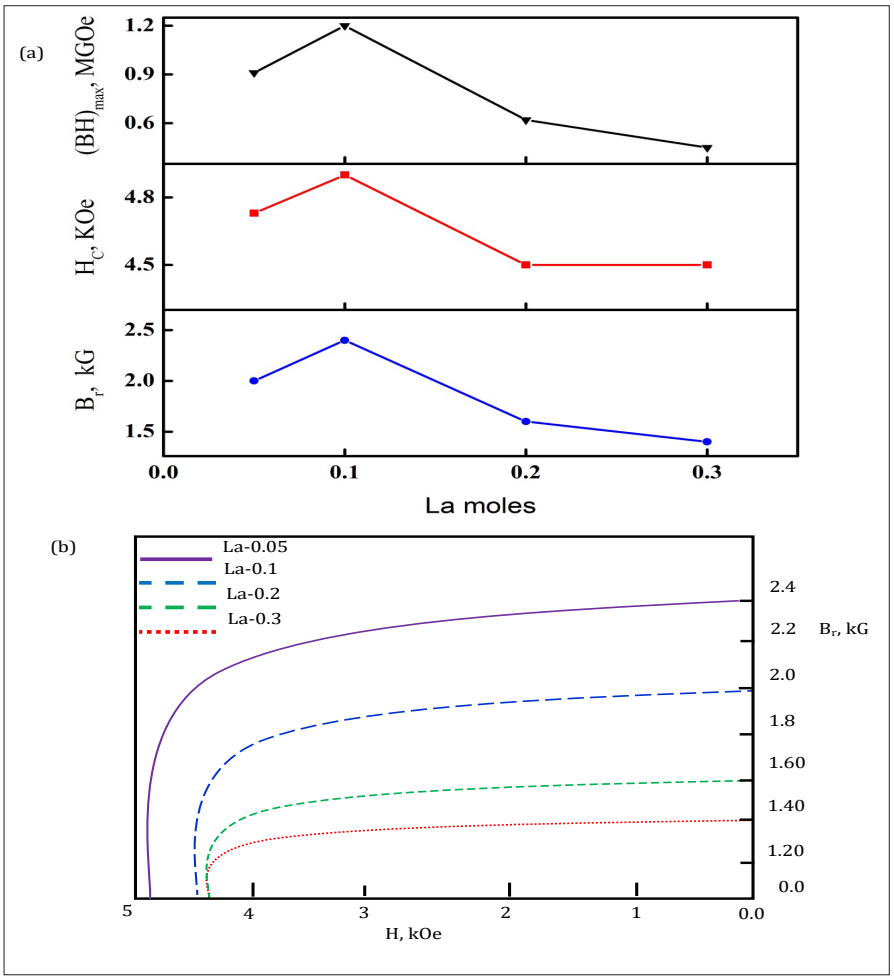

Figure 7: Changes in magnetic properties (a) demagnetization curves (b) as a function of La moles.

Magnetic permeability and susceptibility

The permeability is influenced by the ferrite composition, density, phase structure. The magnetization process which contributes to the permeability of ferrites are known to be spin rotation, domain wall bulging and domain wall displacement [23]. Figure 8a & 8b shows the real and imaginary parts of permeability for La doped ferrites. It shows that initial permeability increases with La_2O_3 doping from 0.05 to 1.0 mole percent and then decline with further La_2O_3 doping. In general, 1.0 mole percent La_2O_3 doped ferrite has a sharp peak spectra compared to all La_2O_3 doped ferrites for both real and imaginary parts of the permeability. The increase in permeability at low frequency is related to the contribution of both domain wall bulging and domain wall displacement in accordance with the reported ferrites [24,25]. It is noticed that the La_2O_3 doped ferrites show a constant permeability behavior over the frequency range 55 to 100GHz. This constant permeability trend suggests compositional stability and equality of fabricated ferrites and known to be the zone of utility of the ferrite. The stability of ferrite is considered as a key parameter for certain applications, such as video recording and broad band pulse transformation, etc. The imaginary part of the permeability curves indicates a peak shift in the frequency range 35 to 55GHz for the ferrites (Figure 8b). This peak shift is related to the intrinsic properties of the grains as well as porosity present in the microstructure. Thus, it can be said that the sintered La_2O_3 doped ferrites have attained maximum density and fine grain size, which, in turn, promoted the permeability of ferrites through the domain wall bulging and domain wall displacement mechanism. In general, the permeability of a ferrite influences by the compositions, process parameters, grain morphology and the nature of phases present in the microstructure.

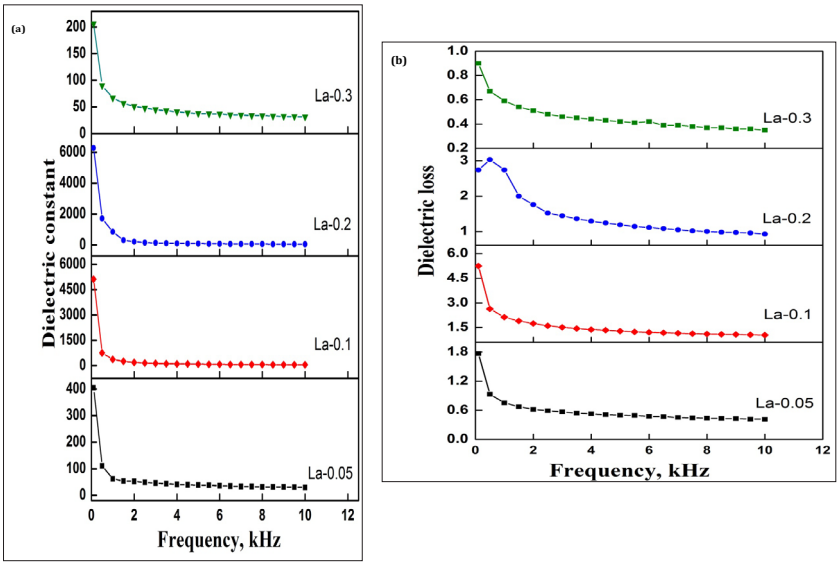

Figure 8: Dielectric properties of La doped ferrites (a) dielectric constant and (b) dielectric loss.

Magnetic susceptibility is an important magnetic parameter to judge the magnetic stability, Curie temperature and phase transformation of the ferrites. It is established that magnetic susceptibility is affected by the grain size, shape, orientation, distribution of grains of ferrites. Figure 8b depicts magnetic susceptibility versus temperature for La_2O_3 doped ferrites. The Hopkinson peak, Hk, [26] appeared at around 430.8 °C for both La_2O_3 doped 0.1 and 0.2 mole percent ferrites. The Curie temperatures, T_c, for 0.1 and 0.2 mole percent ferrites appeared at about 435 °C and 445 °C, respectively. The susceptibility drops rapidly after 435 °C or 445 °C temperature suggesting that ferromagnetic structure has been changed into paramagnetic. In the susceptibility curve, susceptibility changed from the stable paramagnetic state (405 °C) to super-paramagnetic state, where Hopkinson peak attained a maximum value (430.8 °C) because magnetic field anisotropy (H_A) approaches to zero. At the Curie temperature, the susceptibility strongly decreases to zero because spontaneous magnetization vanishes ($J_S \rightarrow 0$) and the ferrite material becomes paramagnetic. It was observed that the Curie temperature in La_2O_3 doped ferrites are 15 °C lower to reported Sr based (459 °C) and Ba based (453 °C) M-type hexa-ferrites [26]. The low Curie temperature in studied ferrites is suspected to the difference in composition and processing method adopted to prepare ferrites.

Thus, based on XRD, SEM, magnetometery, thermomagnetic analysis and dielectric experimental results, it can be said that magnetic properties in isotropic Ba-ferrite depend critically on the microstructural features which become ideal or non-ideal based on the choice of heat treatment temperature and or La content. Magnetic properties owe its origin from the fine grain size, homogenous phase distribution and phase coherency of $BaFe_{12}O_{19}$ phase present in the microstructure. High coercivity (4.9kOe) originates from the reduction in grain size while high B_r from the positive dipole interactions, high grain stacking density as well as density of ferrite. It is worth to mention that magnetic properties in La-0.1 doped samples are better than the reported ferrites produced by electro-spun [27] co-precipitation [28] and powder metallurgy techniques [29]. The magnetic properties in the present alloy can be further enhanced by adding Co content. Isotropic ferrites have similar properties in all directions and can be easily magnetized even at low applied magnetic fields. Moreover, isotropic magnets can be developed with economical process using less cost raw materials which may find their applications in telecommunication and microwave devices. The research work on the development of La doped anisotropic ferrite permanent magnets is in progress and their results will be published in future publication. Research on the development of La doped anisotropic ferrite permanent magnets is in progress and their results will be published in future publication.

Conclusion

Isotropic La-doped ferrites have been synthesized through powder metallurgy technique. Magnetic properties are affected by the alloy constituents elements and sintering or annealing parameters, which in turn, alter the resultant magnet microstructure. Optimum magnetic properties such as H_c=4.9kOe, B_r=2.4kG and $(BH)_{max}$ =1.2MGOe were obtained with La-0.1 added magnets. Optimum magnet reveals 98% decrease for dielectric constant at 10kHz. High coercivity (4.9kOe) originates from the reduction in grain size while high B_r stems from the positive dipole interactions, high grain stacking density as well as density of ferrite. Magnetic properties in present alloy can be further enhanced by employing powder compaction in magnetic field, cold isostatic pressing and spark plasma sintering techniques.

Acknowledgement

This work was supported by the Zhejiang Provincial Natural Science Foundation of China (Grant No. LH19E010001).

References

1. Kools FX, Stoppels D, Othmer K (1993) Encyclopedia of chemical technology. (4th edn), John Wiley and Sons, New York, USA, pp. 381-390.
2. Yeadon AW (2001) Handbook of small electric motors. (1st edn), McGraw Hill Company Inc., USA, pp. 4-134.
3. Nowosielski R, Babilas R, Dercz G, Pajak L, Wrona J (2007) Structure and properties of barium ferrite powder prepared by milling and annealing. Arch of Mater Sci Eng 28(12): 735-742.
4. Pullar RC (2012) Hexagonal ferrites: A review of the synthesis, properties and applications of hexaferrites ceramic. Prog in Mater Sci 57: 1191-1334.
5. Singh VP, Jasrotia R, Kumar R (2018) A current review on the synthesis and magnetic properties of M-type hexaferrite materials. World J of Cond Matt Phys 8: 36-61.
6. Ding J, Chow YY, Wang S, Shi Y (2000) A study on barium ferrite particles prepared by chemical co-precipitation. Mater Res 15(10): 2151-2156.
7. Singh A, Bindra NS, Sing K, Pandey OP, Kotnala RK (2010) Electrical and magnetic properties of rare earth substituted strontium hexaferrite. J Ceramic Proc Res 11 (2): 241-249.
8. Jie L, Huaiwu Z, Yinong L, Ma G, Li Q (2016) Low temperature co-fired Ni-Ti co-substituted barium ferrites. J of composite Mater 50(2): 173-178.
9. Nowosielksi R, Babilas R, Dercez G (2008) Microstruture and magnetic properties of $BaFe_{12}O_{19}$ powder. J Achiev Mater Manuf Eng 27: 51-54.
10. Ding J, Chow YY, Wang S, Shi Y (2000) A study on barium ferrite particles prepared by chemical co-precipitation. Mater Res 15 (10): 2151-2156.
11. Sozeri H, Kucuk I, Ozkan H (2011) Improvement in magnetic properties of La-substituted $BaFe_{12}O_{19}$ particles prepared with an unusually low Fe/ Ba molar ratio. J Magn Magn Mater 323: 1799-1804.
12. Ounnunkad KS (2006) Improving magnetic properties of barium Hexaferrite by La or Pr substitution. Solid State Commun 138: 472-475.
13. Ghzaiel TB, Dhaoui W, Pasko A, Mazaleyrat F (2016) Effect of Non-magnetic and magnetic trivalent ion substitution on Ba-M ferrite properties synthesized by hydrothermal method. J Alloys Comp 671: 245-243.
14. Yang YJ, Liu XS (2014) Microstructure and magnetic properties of La-Cu doped M type strontium ferrites prepared by ceramic process. Adv Perform Mater 29: 232-236.
15. Bhargava GK, Sharma S, Kotnola SRK, Shah J (2013) Electric and dielectric study of cobalt substituted Mg-Mn nano ferrites synthesized by solution combustion techniques. J Molecular Structure 1051(5): 336-344.
16. Wagner KW(1913) On the theory of imperfect dielectrika. Anne De Physics 40: 817.
17. Konstantin AK, John SM, Mohammad Na (2012) Ferromagnetic resonance of micro and nano-sized hexagonal ferrite powders at millimeter waves. J Appl Phys 111: 07E113.
18. Chen Y, Geiler AL, Chen T, Sakai T, Vittoria C, et al. (2007) Low-loss barium ferrite quasi-single-crystals for microwave application. J Appl Phys 101: 09M501.
19. Wang Y, Lianchao L, Chao LH (2008) Magnetic properties and microstructure of La-Substituted Ba-Cr-ferrite powders. Materials Letters 14: 2060-2062.
20. Ounnunkad KS (2006) Improving magnetic properties of barium Hexaferrite by La or Pr substitution. Solid State Commun 138: 472-475.
21. Jacobo SE, Herme C, Bercoff PG (2010) Influence of the iron content on the formation process of substituted Co-Nd strontium hexaferrite prepared by the citrate precursor method. J Alloys Comp 2: 513-515.
22. Maxwell JC (1973) Electricity and Magnetism (2nd edn), Oxford University Press, London.
23. Valenzuela R, Montiel H, Piler GD, Gutierrez MP (2005) Characterization of soft ferromagnetic materials by inductance spectroscopy and magneto impedence. J Magn Magn Matter 294: 239-244 .
24. Debnath N, Rahman MM, Ahmad F (2012) Study of the effect of rare-earth oxide addition on the magnetic and dielectric properties of Sr-hexaferrites. Int J Engg Techn 12: 49-52.
25. Rahaman DM, Mia D, Khan INM (2016) Study the effect of sintering temperature on structural, microstructural, electromagnetic properties of 10% Ca-doped $Mn_{0.6}Zn_{0.4}Fe_2O_4$. J Magn Magn Matter 404: 238-249.
26. Vinnik DA , Tarasova AY, Zherebtsov DA , Gudkova SA, Galimov DM, et al. (2017) Magnetic and structural properties of barium hexaferrite $BaFe_{12}O_{19}$ from various growth techniques. Materials 10: 578.
27. Li CJ, Wang B, Wang JN (2012) Magnetic and microwave absorbing properties of electrospun Ba(1-x)LaxFe12O19 nanofibers. J Magn Magn Matter 324: 1305-1311.
28. Rashad MM, Ibrahim IA (2011) Improvement of the magnetic properties of barium hexaferrite nano powders using modified co-precipitation method. J Magn Magn Matter 323: 2158-2164.
29. Manikandan M, Venkateswaran C (2014) Effect of milling on the synthesis temperature, magnetic and electrical properties of barium hexagonal ferrite. J Magn Magn Matter 358-359: 82-88.